



Advancing the prediction of crystalline phases in glass-ceramics via machine learning

Jiaqian Zhu, Guohao Sun, Linfeng Ding*, Lianjun Wang*

State Key Laboratory for Modification of Chemical Fibers and Polymer Materials, Engineering Research Center of Advanced Glass Manufacturing Technology, Ministry of Education, Donghua University, Shanghai 201620, China



ARTICLE INFO

Keywords:

Glass-ceramics
Lithium aluminosilicate (LAS)
Machine learning (ML)
Crystalline phase prediction

ABSTRACT

Lithium aluminosilicate (LAS) glass-ceramics are widely utilized in diverse application, owing to their outstanding properties such as high transparency, high fracture toughness and ultra-low thermal expansion. The development of LAS glass-ceramics has traditionally relied on the phase diagram to identify primary crystalline phases. However, this approach is limited by constrained composition ranges and unknown heating treatment parameters, hindering the efficient development of high-performance glass-ceramics. In this study, we establish a comprehensive small-scale database of LAS glass-ceramics, comprising 751 samples characterized by 27 compositions, nucleation temperature, nucleation time, crystallization temperature, crystallization time and 13 crystalline phases. We employ five algorithms, i.e. Random Forest (RF), eXtreme Gradient Boosting (XGBoost), Classification and Regression Trees (CART), K-Nearest Neighbors (K-NN) and Multi-Layer Perceptron (MLP) Classifier to predict the potential crystalline phases. Our results demonstrate that RF achieves the best overall performance, with the highest accuracy of 0.8609, the lowest hamming loss of 0.0142, and the highest micro F1 score of 0.9234. This work advances the understanding and prediction of crystalline phases in LAS glass-ceramics, providing valuable insights for the development and optimization of these materials.

1. Introduction

Nanocrystalline lithium aluminosilicate (LAS) glass-ceramics are known for their exceptional properties, including thermal shock resistance, superior vacuum degassing properties, robust mechanical stability, polishability and low helium permeability, etc. [1,2] Owing to this impressive set of properties, LAS glass-ceramics have found diverse applications in various fields. These include their use in kitchen appliances such as cookware and stove windows [3,4], tubes, pipes, bearings and races exposed to high-temperature services [2], mounting systems for precision optics, mirror substrates for astronomical telescopes and X-ray telescope [5,6], accurate measurement benchmarks (calibration artefacts) [5], base blocks for laser gyroscope, lightweight mirrors, range spacers in laser resonators, reflectors, and platforms used in the manufacture of microelectronic devices [7], dental restorations [8–10], and bone replacements [11], etc.

To achieve glass-ceramics with exceptional properties, manufacturers must rigorously control the formation of crystalline phases. These glass-ceramics typically contain at least one type of functional crystalline phase and a residual glass [12], with the composition of oxides and

heating treatment conditions identified as crucial factors. Initially, the LAS phase diagram can suggest primary crystalline phases based on the weight ratio of Li_2O , Al_2O_3 and SiO_2 . The thermo-analysis using differential scanning calorimetry (DSC) is also commonly applied to determine the heating treatment methods. The basic glass is normally heated to a temperature near the glass transition point to induce the development of nuclei, followed by raising the temperature to promote the growth of crystals on the nuclei [13]. Although thermo-analytical studies using DSC have indicated that the optimal temperature window for the crystallization of commercial-grade LAS glass-ceramics falls within the range of 775 to 900 °C [14], the exact heating treatment parameters vary under different experimental conditions [15–17]. In addition, the actual raw material formulations employed in the LAS glass-ceramics production process involve a multitude of additional components, including ZrO_2 , P_2O_5 , Na_2O , K_2O , TiO_2 , MgO , ZnO and BaO [15–17]. Consequently, the prediction of crystalline phases based on LAS phase diagram is limited by its constrained composition ranges. Therefore, the ability to predict potential crystalline phases based on diverse compositions and different heating treatment parameters have become a focal point and challenge in research. Although machine learning (ML)

* Corresponding authors.

E-mail addresses: Linfeng.Ding@dhu.edu.cn (L. Ding), Wanglj@dhu.edu.cn (L. Wang).

algorithms have emerged as an alternative approach for designing new glass-ceramic compositions [18-20], to the best of our knowledge, none have been utilized for crystalline phase prediction tasks.

Fig. 1 illustrates the whole process of the ML experiment. Firstly, we gathered data from published literature [21-48] and patents [49-60], which contributed to dataset A, comprising 449 samples with 27 different compositions, as well as information on nucleation temperature, nucleation time, crystallization temperature, crystallization time, and 9 crystalline phases. We also developed an algorithm to extract information from the LAS phase diagram (**Fig. 2**), which comprised dataset B, consisting of 302 samples characterized by 3 compositions and 7 crystalline phases. By merging dataset A and B, we formed dataset C, which consists of 751 unique samples with 27 compositions and 13 crystalline phases. After data preprocessing, we conducted research using five algorithms, i.e. Random Forest (RF) [61], eXtreme Gradient Boosting (XGBoost) [62], Classification and Regression Trees (CART) [63], K-Nearest Neighbors (K-NN) [64] and Multi-Layer Perceptron (MLP) Classifier [65]. Then we tested models' generalization ability on the small dataset (~30 samples) unseen during the training period. Furthermore, we employed the best-performing model to augment the crystalline phase information within the SciGlass database [66], which may provide valuable reference for future researchers designing new materials. For the purpose of full reproducibility, the codes and datasets utilized in this research are made accessible on Github (<https://github.com/JiaQianZhu/Advancing-the-prediction-of-crystalline-phases-in-glass-ceramics-via-Machine-Learning>).

2. Methodology

2.1. Data collection and preparation

The dataset A used in this work was manually collected from

published literature [21-48] and patents [49-60] on LAS glass-ceramics. The dataset was normalized to ensure that the compositions added up to 100 % in weight percentage. Duplicate entries and entries with incomplete heating treatment parameters were removed. The process yielded crystalline phase data for 449 distinct glasses, characterized by 31 features (27 unique compositions alongside nucleation and crystallization parameters such as temperature and time) and 9 crystalline phases. To incorporate information from the LAS diagram, a self-developed algorithm was employed to culminate dataset B, resulting in 302 data samples characterized by 3 compositions and 7 crystalline phases. After data merging, dataset C was normalized to ensure that the compositions added up to 100 % in weight percentage. The above protocol resulted in crystalline phases data for 751 unique glasses with 31 features (27 different compositions and nucleation temperature, nucleation time, crystallization temperature, crystallization time as the input features) and 13 crystalline phases for model training, testing and further analysis.

2.2. Model training

To train the ML models, the cleaned dataset C was divided into 80:20 proportions for the training and testing sets, respectively. The training set was subjected to 10-fold cross-validation to enable hyperparameter search for an optimal fit. Since machine learning models have different hyper-parameters, they must be chosen appropriately to achieve good generalized model performance. The hyperparameters of the ML models were optimized using the Bayesian optimization-based library, Optuna [67]. To prevent data leakage [68], the test data were kept hidden during the training process and were used only to evaluate the performance of the best model. Due to the presence of class imbalance, micro F1 score was chosen as the loss function for hyper-parameter optimization to evaluate the overall performance of the model. Numpy,

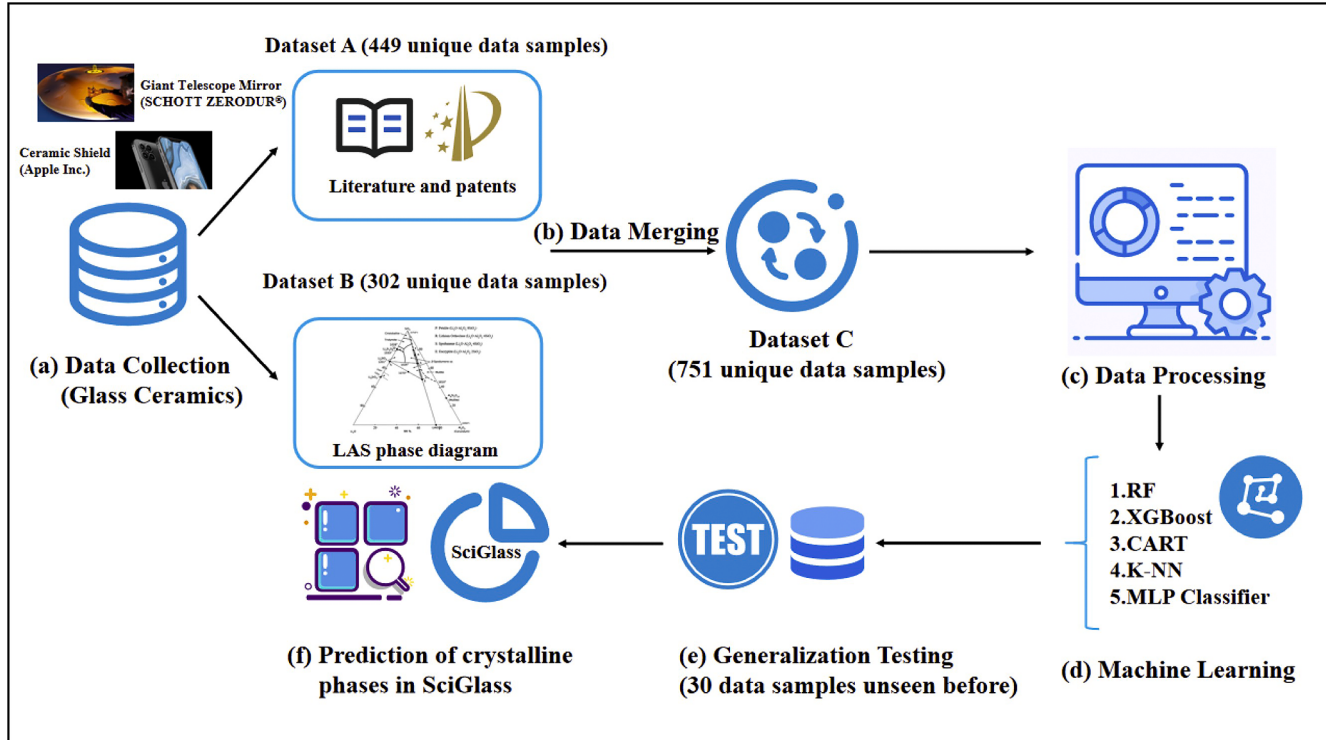


Fig. 1. Illustration of the experiment. We initiated the process with (a) Data Collection, comprising two components: Dataset A sourced from published literature and patents, and Dataset B gathered from the LAS phase diagram. Subsequently, we (b) merged Dataset A and Dataset B to create a consolidated dataset C, resulting in a total of 751 unique data samples. Following that, we carried out (c) Data Processing, ensuring that the sum of the composition weight percentages remained at 100 %. We then employed (d) five machine learning algorithms for the experiment, and (e) assessed their generalization ability on the unseen dataset. Finally, by (f) predicting potential crystalline phases in SciGlass, we provided insights for the future design of LAS glass-ceramics.

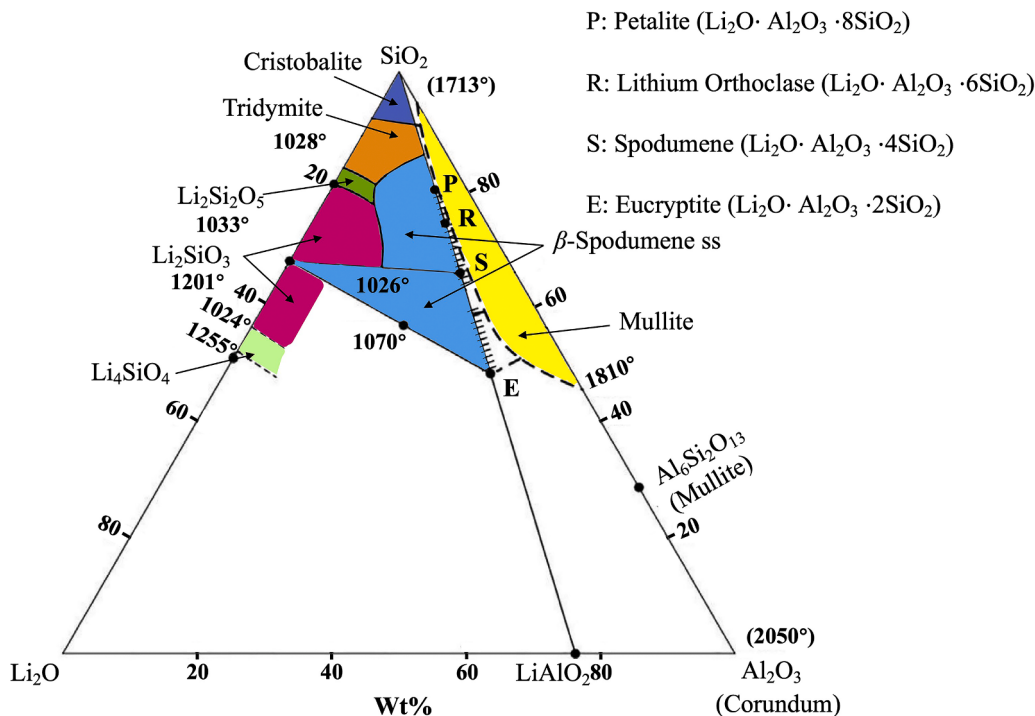


Fig. 2. The phase diagram of $\text{Li}_2\text{O}-\text{Al}_2\text{O}_3-\text{SiO}_2$ (figure modified from the NIST Standard Reference Database 31, No. 499).

Pandas, and Matplotlib [69–71] were used for pre-processing and data visualization.

2.3. Evaluation metrics

To evaluate the model performance, three metrics: accuracy, hamming loss, micro F1 score were applied [72]. Accuracy is one of the simplest and most intuitive metrics for evaluating the performance of a classification model. It represents the proportion of samples that the model correctly predicts compared to the total number of samples. Hamming loss evaluates the fraction of misclassified instance-label pairs, i.e. a relevant label is missed or an irrelevant is predicted. The F1 score is an evaluation metric that comprehensively considers precision and recall, particularly suitable for situations with an imbalanced class distribution. The micro F1 score aggregates performance across all classes by treating each instance equally, making it ideal for handling class imbalance without prioritizing any specific class. Except for hamming loss, which should be closer to 0 for better performance, other metrics are better when closer to 1.

2.4. Shapley additive explanations

The SHAP (SHapley Additive exPlanations) values, estimated using the shap Python module [73], are employed to interpret the predictions generated by the trained models. The SHAP values correspond to each feature in the models, representing the quantity of each chemical element in this specific context. Notably, in classification problems, the SHAP values represent the contribution of each feature to the predicted probability of each class, and exhibit an additive property. This additivity enabled a clear understanding of the contribution of each feature to the final prediction, which holds particular significance for the glass research community.

3. Results and discussion

3.1. Dataset visualization

First, we analyze the compositions, heating treatment parameters and crystalline phases from the literature and patents. Fig. 3 shows the bar chart of glass samples associated with each composition of the training and test sets. The training and test sets have 360 and 89 glasses, respectively. Fig. 4 represents 9 crystalline phases along with their respective frequency in training and test sets, with the top five crystalline phases, identified as LAS glass-ceramics containing β -quartz s.s., β -spodumene, $\text{Li}_2\text{Si}_2\text{O}_5$, Petalite and Li_2SiO_3 . Fig. 5 illustrates the compositions and crystalline phases with their corresponding frequencies extracted from LAS diagram in dataset B.

To further understand the distribution of compositions in dataset A, we plotted the box-plot in Fig. 6, which provides 5 statistical indicators of each composition, that are minimum value, lower quartile (Q1), median (Q2), upper quartile (Q3), and maximum value. We can observe that Al_2O_3 , SiO_2 , Li_2O dominate the majority of weight percentages of glass samples, while the remaining oxides, such as ZrO_2 , P_2O_5 , K_2O , TiO_2 , MgO , ZnO , BaO , vary within ranges of <10 % in weight percentage. Heating treatment conditions are also important factors for crystalline phases formation. In Fig. 7, we plotted the histogram with kernel density estimation to explore the distribution of these four parameters. The nucleation temperature falls between 400°C and 950°C , while crystallization temperature ranges from 660°C to 1160°C (Fig. 7(a)). Additionally, both nucleation time and crystallization time range from 0.16 hour to 6 h (Fig. 7(b)).

3.2. Predictive performance measures

Table 1 presents the predictive performances of ML models on the testing set of dataset C, assessed through accuracy, hamming loss and micro F1 score. We observe that the RF model achieves the best overall performance with the highest accuracy of 0.8609, the lowest hamming loss of 0.0142 and the highest micro F1 score of 0.9234, followed by XGBoost, CART, K-NN and MLP Classifier.

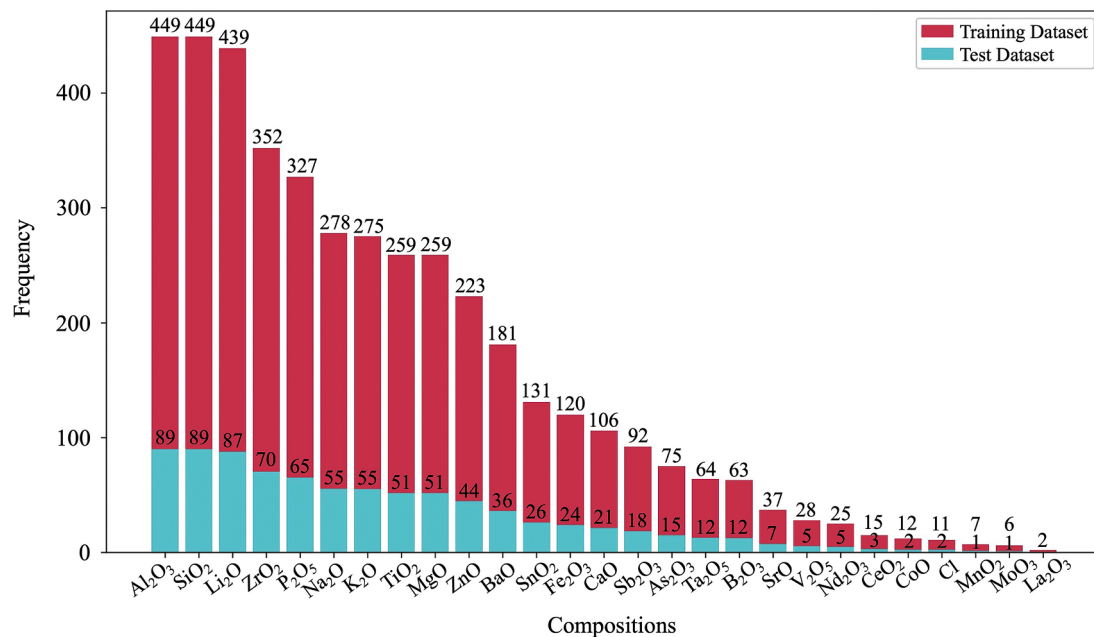


Fig. 3. Compositions versus frequency in dataset A.

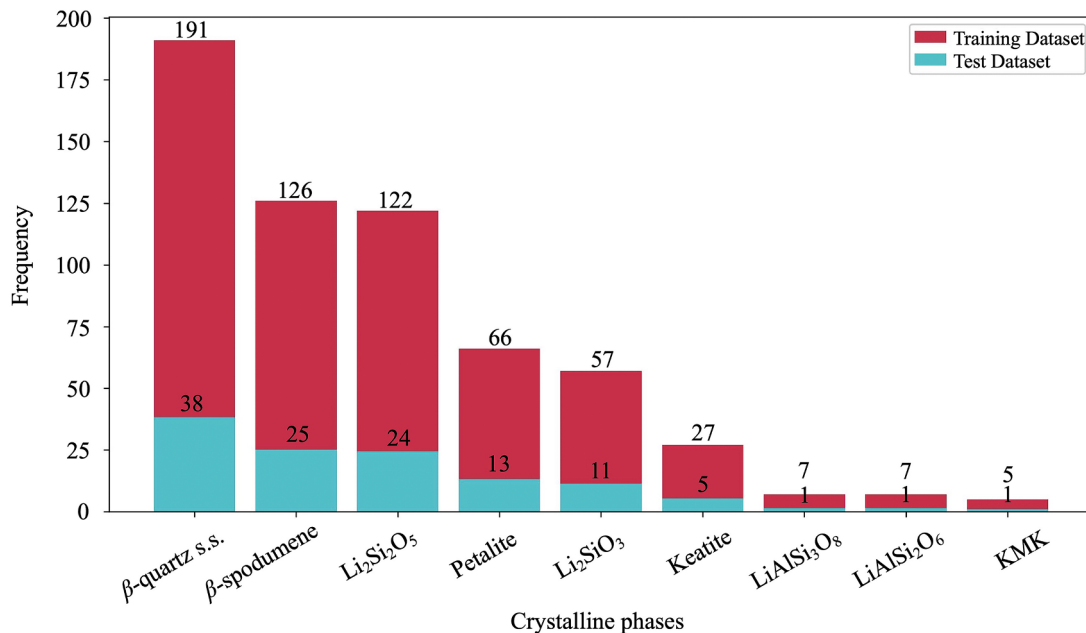


Fig. 4. Crystalline phases versus frequency in dataset A.

3.3. Label correlation analysis

The Label Correlation Heatmap is a valuable data visualization tool used to illustrate correlations among various labels. It is particularly useful for exploring label relationships across the entire dataset, providing a comprehensive understanding of interactions among different labels. When a numerical value is greater than 0, it signifies a positive correlation between the associated labels, indicating that the two labels are more likely to co-occur. Conversely, if the value is <0, it suggests a negative correlation, implying that the occurrence of the two labels together is less likely. The absolute magnitude of the correlation value reflects the strength of the association, with larger values indicating a more pronounced correlation between the labels.

Fig. 8 illustrates the correlation heatmap among different labels

across dataset C, facilitating the analysis of potential relationships between them. The most common commercial LAS glass-ceramics produced at an industrial scale are based on high quartz solid solution (β -quartz s.s.) as the main crystalline phase [1]. According to the reported crystallization mechanism for the low expansion LAS glass-ceramics system, after the nucleation of β -quartz solid solution, a significant amount of metastable high quartz type $\text{LiAlSi}_2\text{O}_6$ precipitates upon increasing the temperature to around 800 °C. This phase subsequently undergoes a transformation to silica-rich spodumene-silica solid solution or keatite at temperatures above 900 °C [14]. Therefore, the probability of simultaneous presence of β -quartz solid solution and β -spodumene in LAS glass-ceramics is quite low, indicating a distinct tendency toward mutual exclusion. This observation is reinforced by the data presented in Fig. 8, where the correlation coefficient between

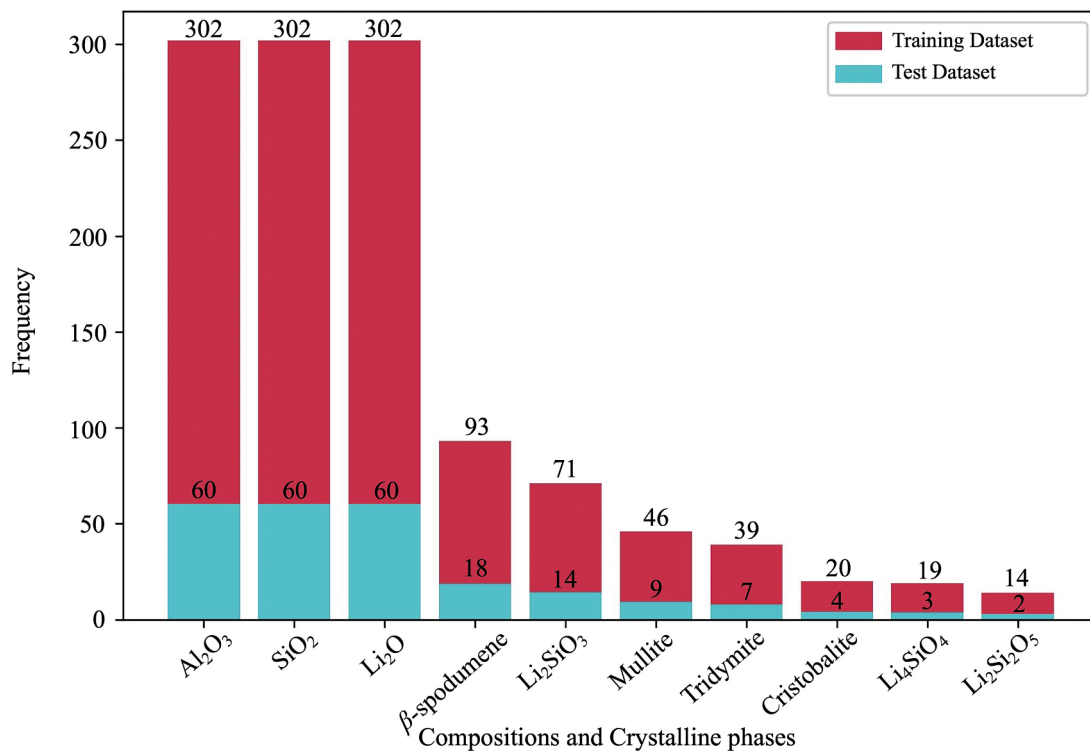


Fig. 5. Compositions and Crystalline phases versus frequency in dataset B.

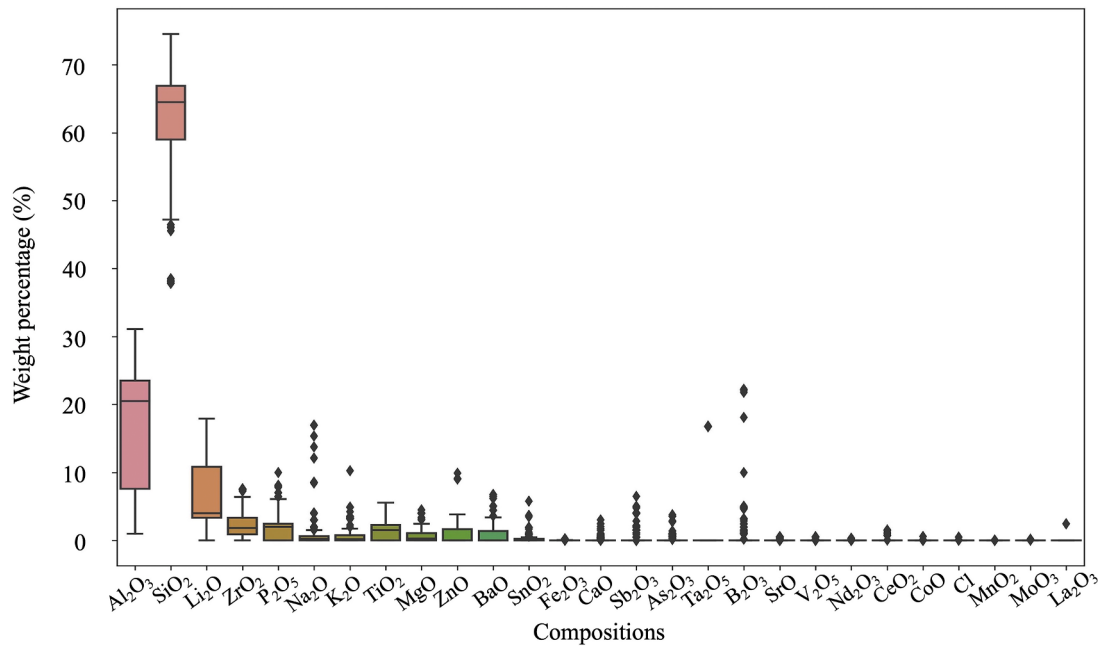


Fig. 6. Box-plot of compositions in dataset A.

β -quartz solid solution and β -spodumene in LAS glass-ceramics is -0.15 . Furthermore, it is noteworthy that petalite undergoes congruent decomposition to form β -spodumene at temperatures around 680 ± 10 °C [74] in LAS glass-ceramics. The correlation coefficient between β -spodumene and petalite in LAS glass-ceramics is -0.18 in Fig. 8, suggesting a negative correlation between these two substances. During the production process of $\text{Li}_2\text{Si}_2\text{O}_5$ in LAS glass-ceramics, the concurrent decomposition of Li_2SiO_3 usually occurs. As $\text{Li}_2\text{Si}_2\text{O}_5$ assumes the role of the predominant crystalline phase, one often observes the coexistence of

minor quantities of other phases, including Li_2SiO_3 , lithium phosphate (Li_3PO_4), cristobalite, and quartz-like phases ($\text{LiAlSi}_2\text{O}_6$ and SiO_2 solid solutions) [75] in LAS glass-ceramics. In addition, we have also identified a correlation coefficient of 0.60 between petalite and $\text{Li}_2\text{Si}_2\text{O}_5$ in LAS glass-ceramics, indicating a potential co-occurrence of these two crystalline phases under specific heat treatment conditions. This finding aligns with experimental observations from DSC measurements on LAS parent glasses, where strong exothermic peaks corresponding to the crystallization of $\text{Li}_2\text{Si}_2\text{O}_5$ at lower temperatures and petalite at higher

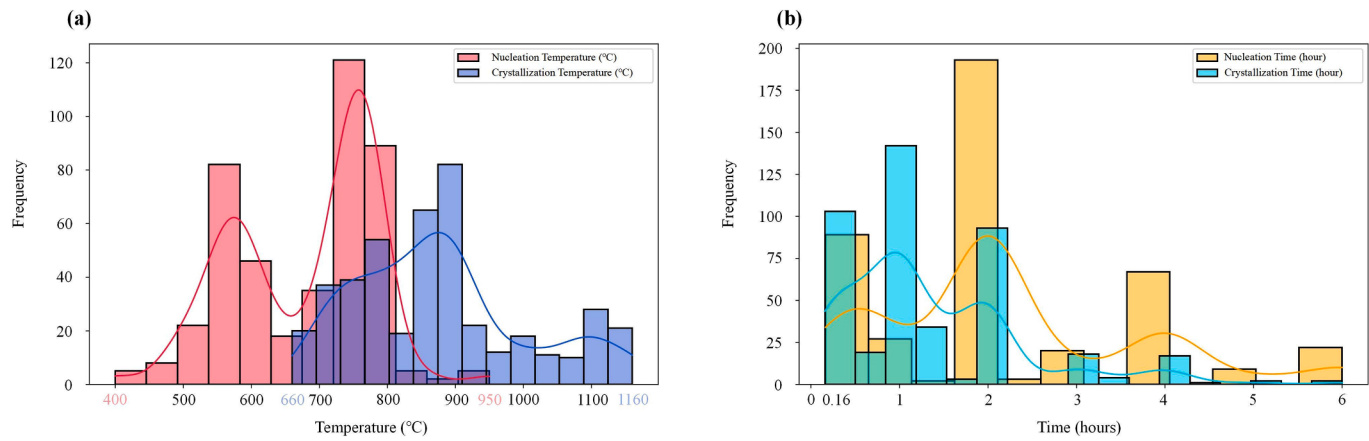


Fig. 7. Histogram with kernel density estimation of (a) heating treatment temperature and (b) heating treatment time in dataset A.

Table 1

Predictive performances of ML models evaluated by accuracy, hamming loss and micro F1 score on the testing set. The upward arrows indicate that the higher the metric the better, whereas the downward arrows indicate the opposite.

Metrics	RF	XGBoost	CART	K-NN	MLP Classifier
Accuracy↑	0.8609	0.8411	0.8411	0.7947	0.7351
Hamming Loss↓	0.0142	0.0153	0.0183	0.0259	0.0265
F1 score (micro)↑	0.9234	0.9171	0.9022	0.8603	0.8531

temperatures coexist. The coexistence of those two crystalline phases has been demonstrated to yield excellent mechanical properties, which find application in the cell-phone industry [76].

3.4. Model interpretation using SHAP

We chose the best-performing model and conducted SHAP analysis for five key crystalline phases. To clearly delineate the impact factors of each process, which include both compositions and heating treatment conditions, each of which is equally crucial, we presented them separately for better clarity.

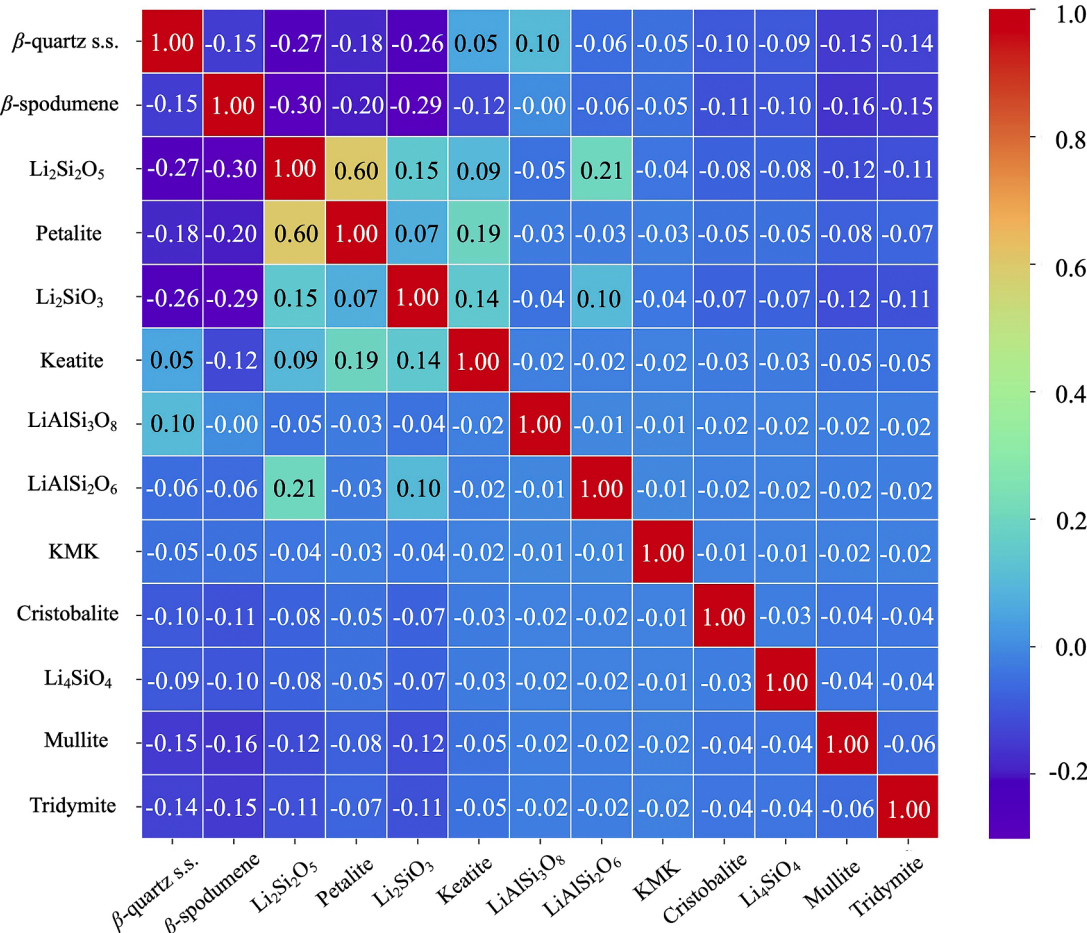


Fig. 8. Label Correlation Heatmap of dataset C.

Analysis of the SHAP plots in Fig. 9 reveals the hierarchy of compositions in predicting desired crystalline phases. For LAS glass-ceramics containing $\text{Li}_2\text{Si}_2\text{O}_5$ (Fig. 9(a)), the top ten oxides in order of importance are P_2O_5 , Li_2O , Al_2O_3 , K_2O , SiO_2 , ZrO_2 , Ta_2O_5 , Na_2O , MgO and TiO_2 . Fig. 9(b) shows the leading ten oxides for LAS glass-ceramics containing Li_2SiO_3 in order of importance: Al_2O_3 , Li_2O , SiO_2 , MgO , Ta_2O_5 , ZrO_2 , TiO_2 , ZnO , K_2O and P_2O_5 . In the investigation of LAS glass-ceramics containing petalite (Fig. 9(c)), we can observe that the top ten oxides are ZrO_2 , Na_2O , P_2O_5 , Li_2O , SiO_2 , TiO_2 , Al_2O_3 , B_2O_3 , MgO and SnO_2 . Moving on to LAS glass-ceramics containing β -quartz s.s., as shown in Fig. 9(d), the ten most important oxides are TiO_2 , Li_2O , MgO , Al_2O_3 , ZrO_2 , ZnO , Sb_2O_3 , K_2O , SnO_2 and SiO_2 . Furthermore, Fig. 9(e) illustrates the intrinsic relationship between LAS glass-ceramics containing β -spodumene and top ten oxides: Al_2O_3 , Li_2O , SiO_2 , P_2O_5 , BaO , ZnO , TiO_2 , K_2O , Na_2O , ZrO_2 .

The oxides mentioned can be categorized into three functional groups based on their roles in glass formation. Li_2O , Al_2O_3 , and SiO_2 act as glass network and crystalline phase formers [77], constructing the primary three-dimensional framework of the glass-ceramics. K_2O , Na_2O , MgO , ZnO and BaO function as glass network modifiers, contributing to charge stabilization of the network formers or modifying the network topology by breaking bridging bonds and lowering the melting

temperature [78]. Additionally, TiO_2 , P_2O_5 , and ZrO_2 serve as nucleating agents, added to the glass batch to promote uniform bulk crystallization. [79]

After analyzing how compositions affect the formation of crystalline phases, we investigate the correlation between heating treatment conditions and desired crystalline phases.

Based on Fig. 10, the heating treatment parameters exhibit commonalities in their effects on LAS glass-ceramics containing $\text{Li}_2\text{Si}_2\text{O}_5$ (Fig. 10(a)), Li_2SiO_3 (Fig. 10(b)) and β -quartz s.s. (Fig. 10(d)) are similar, with nucleation temperature being the dominant factor. By contrast, for LAS glass-ceramics containing β -spodumene (Fig. 10(e)), crystallization temperature is more critical than nucleation temperature. In addition, for LAS glass-ceramics containing Petalite (Fig. 10(c)), the nucleation time plays a more important role than crystallization time.

The SHAP analysis conducted in this study will serve as a valuable tool in refining heating treatment parameters and guiding the formation of specific crystalline phases in the production of glass-ceramics. This will ultimately help to achieve the desired outcomes and enhance the efficiency of the empirical processing methods utilized.

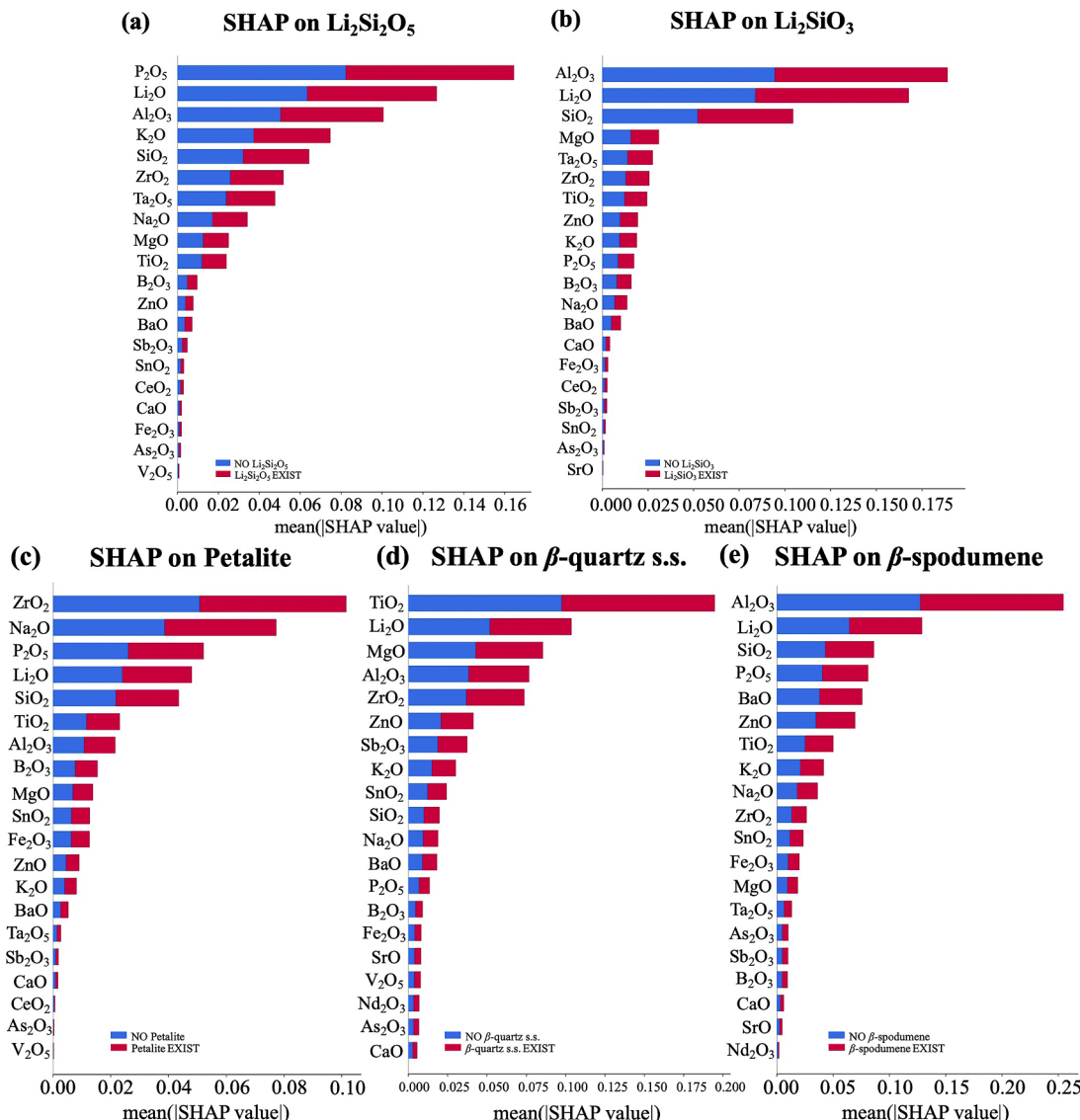


Fig. 9. SHAP analysis between compositions and LAS glass-ceramics containing (a) $\text{Li}_2\text{Si}_2\text{O}_5$, (b) Li_2SiO_3 , (c) Petalite, (d) β -quartz s.s. and (e) β -spodumene.

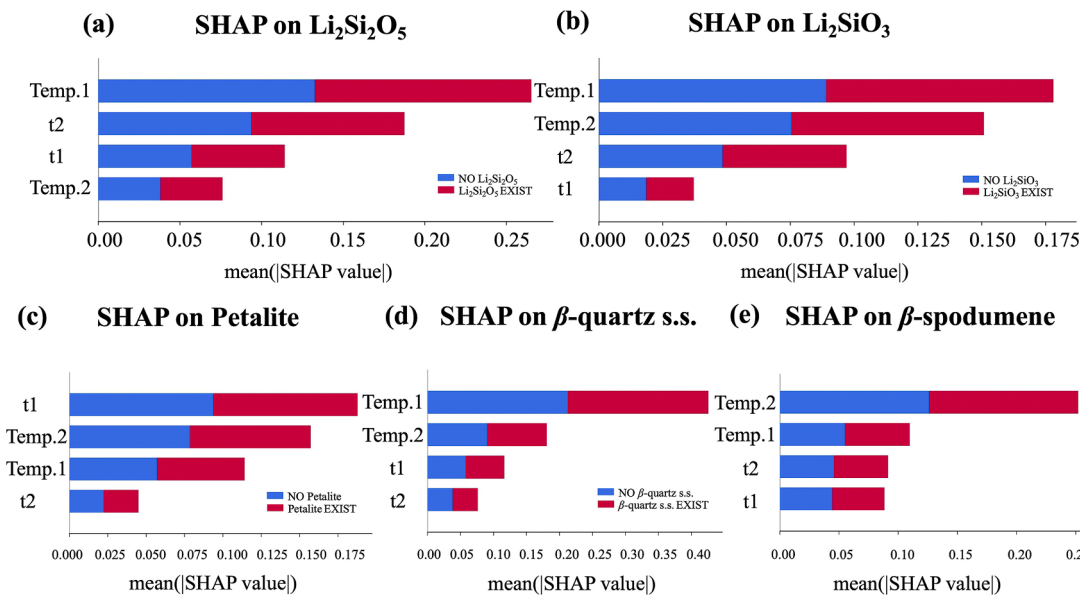


Fig. 10. SHAP analysis between heating treatment conditions and LAS glass-ceramics containing (a) $\text{Li}_2\text{Si}_2\text{O}_5$, (b) Li_2SiO_3 , (c) Petalite, (d) β -quartz s.s. and (e) β -spodumene. Notations: Temp.1 represents nucleation temperature ($^{\circ}\text{C}$), Temp.2 represents crystallization temperature ($^{\circ}\text{C}$), t1 represents nucleation time (hour) and t2 represents crystallization time (hour).

3.5. Generalization testing

The assessment of the generalization ability of trained models is being conducted using a small dataset of approximately 30 glasses that are unseen before [80–95].

Table 2 presents the generalization ability of trained ML models on the unseen dataset, assessed through accuracy, hamming loss and micro F1 score. We observe that the RF model achieves the best overall performance with the highest micro F1 score of 0.8387, followed by XGBoost, MLP Classifier, K-NN and CART. Compared to the results presented in Table 1, the model's generalization performance is inferior to its performance on the test set, which is a typical occurrence in ML. To further enhance the model's generalization capability, a larger composition-heat treatment dataset with more glass-ceramic samples (e.g. 2000) [20] should be built.

3.6. Crystalline phases prediction of SciGlass database

The previous generalization testing confirmed the relatively strong predictive capability of the RF model. Therefore, we have decided to perform potential phase predictions for relevant components within the SciGlass database [66]. After screening, we obtained glass components from the SciGlass database that align with the 31 features used in our experiment, totaling 63,196 entries. We converted all components to weight ratios and then normalized them to ensure that the sum of components in each sample equaled 100 %. We employed our model to predict potential crystalline phases, resulting in a series of generated data that serve as a reference for the future development of LAS glass-ceramics.

4. Summary and conclusions

In this study, we employed machine learning algorithms to train, predict and interpret the compositions, heating treatment parameters and potential crystalline phases of LAS glass-ceramics. First, we collected and complied 449 unique glass samples containing 27 compositions, nucleation temperature, nucleation time, crystallization temperature, crystallization time and 9 crystalline phases from the literature and patents to form dataset A. Then we utilized a self-developed algorithm to extract information from the LAS diagram,

Table 2

Generalization ability of trained ML models evaluated by accuracy, hamming loss and micro F1 score on the unseen dataset. The upward arrows indicate that the higher the metric the better, whereas the downward arrows indicate the opposite.

Metrics	RF	XGBoost	CART	K-NN	MLP Classifier
Accuracy↑	0.7586	0.6207	0.3793	0.5172	0.5172
Hamming Loss↓	0.0265	0.0424	0.0981	0.0610	0.0557
F1 score (micro)↑	0.8387	0.7778	0.5747	0.6462	0.7273

resulting in the creation of dataset B. After merging dataset A and B, we created dataset C, which consists of 751 unique samples with 27 compositions and 13 crystalline phases. We utilized five ML algorithms, i.e. RF, XGBoost, CART, K-NN and MLP Classifier to conduct the experiment. By using small-scale dataset, the RF model achieves a high micro F1 score of 0.9234 and demonstrates strong generalization capability on 30 previously unseen samples. Furthermore, we realized the exploration of potential crystalline phases within the SciGlass database.

CRediT authorship contribution statement

Jiaqian Zhu: Writing – review & editing, Writing – original draft, Visualization, Validation, Software, Methodology, Formal analysis, Data curation. **Guohao Sun:** Writing – review & editing, Supervision, Resources, Methodology, Investigation, Funding acquisition. **Linfeng Ding:** Writing – review & editing, Writing – original draft, Visualization, Validation, Supervision, Methodology, Investigation, Funding acquisition, Conceptualization. **Lianjun Wang:** Writing – review & editing, Supervision, Resources, Investigation, Funding acquisition.

Declaration of competing interest

The authors declare that they have no known competing financial interests or personal relationships that could have appeared to influence the work reported in this paper.

Data availability

Data will be made available on request.

Acknowledgments

The authors gratefully acknowledge financial support from the National Natural Science Foundation of China (U22A20125, 52102002, 62202095), Shanghai Municipal Natural Science Foundation (22ZR1400400), Shanghai Pujiang Program (22PJD002), Fundamental Research Funds for the Central Universities (2232024G-07, 22D111210, 22D111207), and Shanghai Science and Technology Commission (22YF1401100).

References

- [1] H. Bach, D. Krause, *Low Thermal Expansion Glass Ceramics*, 2nd ed., Springer Science & Business Media, Berlin, 2005.
- [2] S.D. Stoekey, Catalyzed crystallization of glass in theory and practice, *Ind. Eng. Chem.* 51 (1959) 805–808, <https://doi.org/10.1021/ie50595a022>.
- [3] G.H. Beall, Milestones in glass-ceramics: a personal perspective, *Int. J. Appl. Glas. Sci.* 5 (2014) 93–103, <https://doi.org/10.1111/ijag.12063>.
- [4] W. Höland, G.H. Beall, *Glass-ceramic Technology*, 2nd ed., Wiley, Hoboken, 2019.
- [5] E.D. Zanotto, A bright future for glass-ceramic, *Am. Ceram. Soc. Bull.* 89 (2010) 19–27.
- [6] T. Döhring, R. Jedamzik, A. Thomas, et al., Forty years of ZERODUR® mirror substrates for astronomy: review and outlook, *Adv. Opt. Mech. Technol. Telesc. Instrum.* 7018 (2008) B183, <https://doi.org/10.1117/12.788936>.
- [7] N. Reisert, Application and machining of 'Zerodur' for optical purposes, *Opt. Fabr. Test.* 1400 (1991) 171–177, <https://doi.org/10.1117/12.47835>.
- [8] L.R. Sakaguchi, J.M. Powers, *Craig's Restorative Dental Materials*, 13th ed., Elsevier, Netherland, 2012.
- [9] M. Gehrt, S. Wolfart, N. Rafai, et al., Clinical results of lithium disilicate crowns after up to 9 years of service, *Clin. Oral Invest.* 17 (2013) 275–284, <https://doi.org/10.1007/s000784-012-0700-x>.
- [10] P.C. Guess, R.C. Zavanelli, N. Silvia, et al., Monolithic CAD/CAM lithium disilicate versus veneered Y-TZP crowns: comparison of failure modes and reliability after fatigue, *Int. J. Prosthodont.* 23 (2010) 434–442, <https://doi.org/10.1111/j.1365-263X.2010.01059.x>.
- [11] Z. Strnad, *Glass-ceramic Materials Liquid Phase separation, Nucleation and Crystallization in Glasses*, 1st ed., Elsevier, New York, 1986.
- [12] J. Deubener, M. Allix, M.J. Davis, et al., Updated definition of glass-ceramics, *J. Non-Cryst. Solids* 501 (2018) 3–10, <https://doi.org/10.1016/j.jnoncrysol.2018.01.033>.
- [13] P.W. McMillan, *Glass-Ceramics*, 2nd ed., Academic Press, Cambridge, 1964.
- [14] C. Venkateswaran, H. Sreemoolanadhan, V. Rahul, Lithium aluminosilicate (LAS) glass-ceramics: a review of recent progress, *Int. Mater. Rev.* 67 (2022) 620–657, <https://doi.org/10.1080/09506608.2021.1994108>.
- [15] G.H. Beall, H.D. Boek, A.M. Mayolet, et al., *Fusion Formable Lithium Aluminosilicate Glass Ceramic*, Google Patents, 2016.
- [16] E. Molieres, M. Comte, *Transparent, Essentially Colorless, Tin-Fined Las Glass-Ceramics with Improved Microstructure and Thermal Expansion Properties*, Google Patents, 2021.
- [17] L. Wondraczek, P. Pradeau, Transparent hafnia-containing β-quartz glass ceramics: nucleation and crystallization behavior, *J. Am. Ceram. Soc.* 91 (2008) 1945–1951, <https://doi.org/10.1111/j.1551-2916.2008.02373.x>.
- [18] D.R. Cassar, S.M. Mastelini, T. Botari, et al., Predicting and interpreting oxide glass properties by machine learning using large datasets, *Ceram. Int.* 47 (2021) 23958–23972, <https://doi.org/10.1016/j.ceramint.2021.05.105>.
- [19] J.C. Mauro, A. Tandia, K.D. Vargheese, et al., Accelerating the design of functional glasses through modeling, *Chem. Mater.* 12 (2016) 4267–4277, <https://doi.org/10.1021/acscchemmater.6b01054>.
- [20] J. Zhu, L. Ding, G. Sun, et al., Accelerating design of glass substrates by machine learning using small-to-medium datasets, *Ceram. Int.* 50 (2024) 3018–3025, <https://doi.org/10.1016/j.ceramint.2023.11.048>.
- [21] S. Fujita, A. Sakamoto, M. Tomozawa, Behavior of water in glass during crystallization, *J. Non-Cryst. Solids* 320 (2003) 1–3, <https://doi.org/10.1016/j.jnoncrysol.2018.01.033>.
- [22] A. Sakamoto, S. Yamamoto, Fabrication of Li2O-Al2O3-SiO2 glass-ceramic ferrules by precision drawing of crystallized preforms, *J. Mater. Sci.* 38 (2003) 2305–2310, <https://doi.org/10.1023/A:1023920110755>.
- [23] H. Savabieh, P. Alizadeh, Y. Dasilva, et al., Investigation of dielectric properties and microstructure of sintered 13.2Li2O-67.6SiO2-14.49Al2O3-3.3TiO2-0.4BaO-0.97ZnO glass-ceramics, *J. Eur. Ceram. Soc.* 37 (2017) 631–639, <https://doi.org/10.1016/j.jeurceramsoc.2016.09.009>.
- [24] V.O. Soares, A.M. Rodrigues, Improvements on sintering and thermal expansion of lithium aluminum silicate glass-ceramics, *Ceram. Int.* 46 (2020) 17430–17436, <https://doi.org/10.1016/j.ceramint.2020.04.037>.
- [25] C. Venkateswaran, H. Sreemoolanadhan, B. Pant, et al., Processing Li2O-Al2O3-SiO2 (LAS) glass-ceramic with and without P2O5 through bulk and sintering route, *J. Non-Cryst. Solids* 550 (2020) 120289, <https://doi.org/10.1016/j.jnoncrysol.2020.120289>.
- [26] A. Lipatieve, S. Fedotov, S. Lotarev, et al., Direct laser writing of depressed-cladding waveguides in extremely low expansion lithium aluminosilicate glass-ceramics, *Opt. Laser Technol.* 138 (2021) 106846, <https://doi.org/10.1016/j.optlastec.2020.106846>.
- [27] G. Yang, P. Lu, L. Zhao, et al., Dynamic response of a Li2O-Al2O3-SiO2 transparent glass-ceramic under shock compression, *J. Eur. Ceram. Soc.* 42 (2022) 5074–5078, <https://doi.org/10.1016/j.jeurceramsoc.2022.05.018>.
- [28] J. Zhang, J. Huang, Y. Yu, et al., Effect of substitution of ZrO2 by SnO2 on crystallization and properties of environment-friendly Li2O-Al2O3-SiO2 system (LAS) glass-ceramics, *Ceram. Int.* 48 (2022) 21355–21361, <https://doi.org/10.1016/j.ceramint.2022.04.101>.
- [29] V.O. Soares, A.M. Rodrigues, Improvements on sintering and thermal expansion of lithium aluminum silicate glass-ceramics, *Ceram. Int.* 46 (2020) 17430–17436, <https://doi.org/10.1016/j.ceramint.2020.04.037>.
- [30] C. Ji, L. Li, W. Gao, et al., Influence of Al2O3/SiO2 ratio in multicomponent LNAs glasses and glass-ceramics on the crystallization behavior, microstructure and mechanical performance, *Ceram. Int.* 49 (2023) 10652–10662, <https://doi.org/10.1016/j.ceramint.2022.11.253>.
- [31] W. She, W. Xu, T. Yang, et al., Microstructure and crystallization behavior of Na2O-Al2O3-SiO2 glass-ceramics with MgO additions, *Ceram. Int.* 49 (2023) 22644–22653, <https://doi.org/10.1016/j.ceramint.2023.05.012>.
- [32] T. Zhang, Z. Zhang, J. Han, et al., The structure and properties of chemical strengthened monolithic lithium disilicate glass ceramics with various P2O5 contents, *J. Non-Cryst. Solids* 588 (2022) 121626, <https://doi.org/10.1016/j.jnoncrysol.2022.121626>.
- [33] A.V. DeCeanne, A.L. Fry, C.J. Wilkinson, et al., Experimental analysis and modeling of the Knoop hardness of lithium disilicate glass-ceramics containing lithium tantalum as a secondary phase, *J. Non-Cryst. Solids* 585 (2022) 121540, <https://doi.org/10.1016/j.jnoncrysol.2022.121540>.
- [34] K. Laczka, K. Cholewa-Kowalska, M. Sroda, et al., Glass-ceramics of LAS (Li2O-Al2O3-SiO2) system enhanced by ion-exchange in KNO3 salt bath, *J. Non-Cryst. Solids* 428 (2015) 90–97, <https://doi.org/10.1016/j.jnoncrysol.2015.08.003>.
- [35] L. Arnault, M. Gerland, A. Rivière, Microstructural study of two LAS-type glass-ceramics and their parent glass, *J. Mater. Sci.* 35 (2000) 2331–2345, <https://doi.org/10.1023/A:1004716018522>.
- [36] A. Arvind, R. Kumar, M.N. Deo, et al., Preparation, structural and thermo-mechanical properties of lithium aluminum silicate glass-ceramics, *Ceram. Int.* 35 (2009) 1661–1666, <https://doi.org/10.1016/j.ceramint.2008.07.019>.
- [37] M. Chen, F. He, J. Shi, et al., Low Li2O content study in Li2O-Al2O3-SiO2 glass-ceramics, *J. Eur. Ceram. Soc.* 39 (2019) 4988–4995, <https://doi.org/10.1016/j.jeurceramsoc.2019.07.032>.
- [38] D. Feng, Y. Zhu, F. Li, et al., Influence investigation of CaF2 on the LAS based glass-ceramics and the glass-ceramic/diamond composites, *J. Eur. Ceram. Soc.* 36 (2016) 2579–2585, <https://doi.org/10.1016/j.jeurceramsoc.2016.03.020>.
- [39] M. Gan, C. Wong, Properties of selective laser melted spodumene glass-ceramic, *J. Eur. Ceram. Soc.* 37 (2017) 4147–4154, <https://doi.org/10.1016/j.jeurceramsoc.2017.04.060>.
- [40] M. Laczka, K. Laczka, K. Cholewa-Kowalska, et al., Mechanical properties of a lithium disilicate strengthened lithium aluminosilicate glass-ceramic, *J. Am. Ceram. Soc.* 97 (2014) 361–364, <https://doi.org/10.1111/jace.12780>.
- [41] P. Lu, Y. Zheng, J. Cheng, et al., Effect of La2O3 addition on crystallization and properties of Li2O-Al2O3-SiO2 glass-ceramics, *Ceram. Int.* 39 (2013) 8207–8212, <https://doi.org/10.1016/j.ceramint.2013.04.004>.
- [42] R. Mishra, M. Goswami, A. Dixit, et al., Study on thermophysical properties and phase evolution in Nd doped Li2O-Al2O3-SiO2 glass nucleated by multiple nucleating agents, *J. Non-Cryst. Solids* 447 (2016) 66–73, <https://doi.org/10.1016/j.jnoncrysol.2016.05.035>.
- [43] A.M. Hu, M. Li, D. Mao, Controlled crystallization of glass-ceramics with two nucleating agents, *Mater. Charact.* 60 (2009) 1529–1533, <https://doi.org/10.1016/j.matchar.2009.09.001>.
- [44] A. Wei, Z. Liu, F. Zhang, et al., Thermal expansion coefficient tailoring of LAS glass-ceramic for anodic bondable low temperature co-fired ceramic application, *Ceram. Int.* 46 (2020) 4771–4777, <https://doi.org/10.1016/j.ceramint.2019.10.209>.
- [45] Q. Zhang, Y. Zhu, Z. Li, Performance investigation of Li2O-Al2O3-4SiO2 based glass-ceramics with B2O3, Na3AlF6 and Na2O fluxes, *J. Non-Cryst. Solids* 358 (2012) 680–686, <https://doi.org/10.1016/j.jnoncrysol.2011.11.003>.
- [46] H.A. Lutpi, H. Mohamad, T.K. Abdulla, et al., Effect of ZnO on the structural, physio-mechanical properties and thermal shock resistance of Li2O-Al2O3-SiO2 glass-ceramics, *Ceram. Int.* 48 (2022) 7677–7686, <https://doi.org/10.1016/j.ceramint.2021.11.315>.
- [47] J. Liu, Q. Wang, Z. Zhang, et al., Investigation on crystallization behavior, structure, and properties of Li2O-Al2O3-SiO2 glasses and glass-ceramics with co-doping ZrO2/P2O5, *J. Non-Cryst. Solids* 576 (2022) 121226, <https://doi.org/10.1016/j.jnoncrysol.2021.121226>.
- [48] N. Zhang, M. Li, X. Dong, et al., The effect of phase formation on biomechanical and biological performance of Li2O-Al2O3-SiO2 glass-ceramics, *Ceram. Int.* 48 (2022) 10187–10194, <https://doi.org/10.1016/j.ceramint.2021.12.230>.
- [49] P. Lespade, G.J.C. Larnac, P. Peres, et al., Fibre-Reinforced Ceramic Composite Material Has Silicon Carbide Type Fibres in Aluminosilicate Ceramic or Glass-Ceramic Matrix, Google Patents, 1993.
- [50] N. Shimatani, A. Sakamoto, Transparent Glass Ceramic Composition for Front windows, Contains Beta-Quartz Solid Silicon Which is precipitated, and has Specific Mean Linear Heating Coefficient of Expansions, Google Patents, 2000.
- [51] C.C. Smith, R.W. Pfizenmaier, Coloured Glass Ceramics Having a Primary Crystal Phase Selected from Beta-Quartz Solid Solution and Beta-Spodumene Solid Solution, Google Patents, 1996.
- [52] R.O. VOSS, High Strength Unitary Glass-Ceramic Article Strengthened By Sodium Ion-Exchange on Surface of Beta-Spodumene Phase, Google Patents, 1978.
- [53] R.W. Pfizenmaier, Ivory-Coloured Opaque Glass Ceramic Material Having Beta-Spodumene Primary Crystal Phase, Google Patents, 1996.

- [54] S. Nakane, Setter for Heat-Processing Glass Substrate for Flat Panel Display, is Made of Glass Ceramic or Ceramic Sintered Compact, and the To-Be-Heated Glass Substrate is Mounted On the Mounting Surface of Setter and Heat-Processed, Google Patents, 2023.
- [55] C.R. Toyota, L. Dev, Lithium Alumino Silicate Glass Ceramic, Google Patents, 1974.
- [56] R.G. Ackerman, B.R. Karstetter, High Strength Unitary Glass-Ceramic Article Strengthened by Potassium Ion-Exchange on Surface of Beta-Spodumene Phase, Google Patents, 1978.
- [57] T. Matano, A. Sakamoto, Lithium Oxide-Alumina-Silica Group Glass Ceramic Material for Optical Coupler, Contains Iron Oxide and Beta-Quartz Solid Solution, and Has Preset Thermal Expansion Coefficient and Ultraviolet Light Transmission Rate, Google Patents, 2002.
- [58] L. Wondraczek, Developing a Blue Transparent Glass ceramic, Useful to Make Articles e.g. Hotplate, Containing a Solid Solution of Beta-Quartz as Main Crystalline Phase, Comprises Heat Treatment of a Lithium Aluminosilicate Glass for Ceramization, Google Patents, 2008.
- [59] K G, Nippon (NIGA-C), Low-Expansion High Strength Glass Ceramics, Google Patents, 1970.
- [60] A.R.E. Carre, A. Andrieu, D.L.G. Ricoult, et al., Glass Or Glass-Ceramic Cookware With Reduced Adherence For Food, Google Patents, 1994.
- [61] L. Breiman, Random forests, Mach. Learn. 45 (2001) 5–32, <https://doi.org/10.1023/A:1010933404324>.
- [62] T. Chen, G. Carlos, XGBoost: a scalable tree boosting system, in: Proceedings of the 22nd ACM SIGKDD International Conference on Knowledge Discovery and Data Mining, 2016, pp. 785–794, <https://doi.org/10.1145/2939672.2939785>.
- [63] A. Clare, R.D. King, Knowledge discovery in multi-label phenotype data, Lect. Notes Comput. Sci. 2168 (2001) 42–53, https://doi.org/10.1007/3-540-44794-4_4.
- [64] M. Zhang, Z. Zhou, ML-kNN: a lazy learning approach to multi-label learning, Pattern Recognit. 40 (2007) 2038–2048, <https://doi.org/10.1016/j.patcog.2006.12.019>.
- [65] K. Hornik, M. Stinchcombe, H. White, Multilayer feedforward networks are universal approximators, Neural Netw. 2 (1989) 359–366, [https://doi.org/10.1016/0893-6080\(89\)90020-8](https://doi.org/10.1016/0893-6080(89)90020-8).
- [66] epam/SciGlass, EPAM systems. <https://github.com/epam/SciGlass>, 2019. (Accessed 18 August 2024).
- [67] E.O. Bernhardt, Über die Mikrohärte der Feststoffe im Grenzbereich des Kick'schen „Ähnlichkeitssatzes, Int. J. Mater. Res. 33 (1941) 135–144, <https://doi.org/10.1515/ijmr-1941-330305>.
- [68] S. Kaufman, S. Rosset, C. Perlich, et al., Leakage in data mining: formulation, detection, and avoidance, ACM Trans. Knowl. Discov. Data 6 (2012) 15, <https://doi.org/10.1145/2382577.2382579>.
- [69] C.R. Harris, K.J. Millman, S.J. van der Walt, et al., Array programming with NumPy, Nature 585 (2020) 357–362, <https://doi.org/10.1038/s41586-020-2649-2>.
- [70] J. Reback, W. McKinney, jbrockmendel, et al., pandas-dev/pandas: Pandas 1.2.0rc0, (2020). <https://doi.org/10.5281/zenodo.4311557>.
- [71] J.D. Hunter, Matplotlib: a 2D graphics environment, Comput. Sci. Eng 9 (2007) 90–95, <https://doi.org/10.1109/MCSE.2007.55>.
- [72] M. Zhang, Z. Zhou, A review on multi-label learning algorithms, IEEE Trans. Knowl. Data Eng. 26 (2014) 1819–1837, <https://doi.org/10.1109/TKDE.2014.2649.2>.
- [73] S.M. Lundberg, G. Erion, H. Chen, et al., From local explanations to global understanding with explainable AI for trees, Nat. Mach. Intell. 2 (2020) 56–67, <https://doi.org/10.1038/s42256-019-0138-9>.
- [74] R. Roy, D.M. Roy, E.F. Osborn, Compositional and stability relationships among the lithium aluminosilicates: eucryptite, spodumene, and petalite, J. Am. Ceram. Soc. 33 (1950) 152–159, <https://doi.org/10.1111/j.1151-2916.1950.tb12780.x>.
- [75] K. Hurle, J. Lubauer, R. Belli, et al., On the assignment of quartz-like LiAlSi₂O₆-SiO₂ solid solutions in dental lithium silicate glass-ceramics: virgilite, high quartz, low quartz or stuffed quartz derivatives? Dent. Mater. 38 (2022) 1558–1563, <https://doi.org/10.1016/j.dental.2022.07.009>.
- [76] J.D. Musgraves, J. Hu, L. Calvez, Springer Handbook of Glass, 1st ed, Springer Nature Switzerland AG, Switzerland, 2019.
- [77] J. Jiusti, E.D. Zanotto, S.A. Feller, et al., Effect of network formers and modifiers on the crystallization resistance of oxide glasses, J. Non-Cryst. Solids 550 (2020) 120359, <https://doi.org/10.1016/j.jnoncrysol.2020.120359>.
- [78] J.C. Mauro, Statistics of modifier distributions in mixed network glasses, J. Chem. Phys. 138 (2013) 12A522, <https://doi.org/10.1063/1.4773356>.
- [79] K. Das, S. Raha, D. Chakraborty, et al., Effect of Nucleating Agents on the Crystallization and Microstructural Characteristics of Blast Furnace Slag Derived Glass-Ceramics, T. Indian Ceram. Soc. 71 (2012) 137–142, <https://doi.org/10.1080/0371750X.2012.738482>.
- [80] G.H. Beall, Design and properties of glass-ceramics, Annu. Rev. Mater. Sci. 22 (1992) 91–119, <https://doi.org/10.1146/annurev.ms.22.080192.000515>.
- [81] M. Dressler, B. Rüdinger, J. Deubener, Crystallization kinetics in a lithium aluminosilicate glass using SnO₂ and ZrO₂ additives, J. Non-Cryst. Solids 389 (2014) 60–65, <https://doi.org/10.1016/j.jnoncrysol.2014.02.008>.
- [82] G.H. Beall, L.R. Pincney, Nanophase glass-ceramics, J. Am. Ceram. Soc. 82 (2004) 5–16, <https://doi.org/10.1111/j.1151-2916.1999.tb01716.x>.
- [83] L. Cormier, O. Dargaud, G. Calas, et al., Zr environment and nucleation role in aluminosilicate glasses, Mater. Chem. Phys. 152 (2015) 41–47, <https://doi.org/10.1016/j.matchemphys.2014.12.008>.
- [84] L.H. Aliyah, A.T. Katrina, M. Hasmaliza, Preliminary study on the development of new composition lithium aluminosilicate glass ceramic, Mater. Today Proc. 17 (2019) 946–952, <https://doi.org/10.1016/j.matpr.2019.06.446>.
- [85] L. Lilenstein, Q. Fu, B.R. Wheaton, et al., Kinetic study on lithium-aluminosilicate (LAS) glass-ceramics containing MgO and ZnO, Ceram. Int. 40 (2014) 11657–11661, <https://doi.org/10.1016/j.ceramint.2014.03.171>.
- [86] M. Guedes, A.C. Ferro, J.M.F. Ferreira, Nucleation and crystal growth in commercial LAS compositions, J. Eur. Ceram. Soc. 21 (2001) 1187–1194, [https://doi.org/10.1016/S0955-2219\(00\)00333-2](https://doi.org/10.1016/S0955-2219(00)00333-2).
- [87] A. Kumar, A. Chakrabarti, M.S. Shekhawat, et al., Transparent ultra-low expansion lithium aluminosilicate glass-ceramics: crystallization kinetics, structural and optical properties, Thermochim. Acta 676 (2019) 155–163, <https://doi.org/10.1016/j.tca.2019.04.006>.
- [88] V. Maier, G. Müller, Mechanism of oxide nucleation in lithium aluminosilicate glass-ceramics, J. Am. Ceram. Soc. 70 (1987) 176–178, <https://doi.org/10.1111/j.1151-2916.1987.tb0517.x>.
- [89] F. Siebers, E. Weiss, K. Schoenberger, et al., Transparent Low-Color Lithium Aluminum Silicate Glass Ceramic and the Use Thereof, Google Patents, 2016.
- [90] G.H. Beall, H.D. Boek, A.M. Mayolet, et al., Fusion Formable Lithium Aluminosilicate Glass Ceramic, Google Patents, 2016.
- [91] W. Höland, V. Rheinberger, E. Apel, et al., Principles and phenomena of bioengineering with glass-ceramics for dental restoration, J. Eur. Ceram. Soc. 27 (2007) 1521–1526, <https://doi.org/10.1016/j.jeurceramsoc.2006.04.101>.
- [92] E. Apel, C. Hoen, V. Rheinberger, et al., Influence of ZrO₂ on the crystallization and properties of lithium disilicate glass-ceramics derived from a multi-component system, J. Eur. Ceram. Soc. 27 (2006) 1571–1577, <https://doi.org/10.1016/j.jeurceramsoc.2006.04.103>.
- [93] P. Goharian, A. Nemati, M. Shabanian, et al., Properties, crystallization mechanism and microstructure of lithium disilicate glass-ceramic, J. Non-Cryst. Solids 356 (2010) 208–214, <https://doi.org/10.1016/j.jnoncrysol.2009.11.015>.
- [94] F. Wang, J. Gao, H. Wang, et al., Flexural strength and translucent characteristics of lithium disilicate glass-ceramics with different P2O5 content, Mater. Des. 31 (2010) 3270–3274, <https://doi.org/10.1016/j.matesdes.2010.02.013>.
- [95] P. Zhang, X. Li, J. Yang, et al., Effect of heat treatment on the microstructure and properties of lithium disilicate glass-ceramics, J. Non-Cryst. Solids 402 (2014) 101–105, <https://doi.org/10.1016/j.jnoncrysol.2014.05.023>.